Beyond the visible: molecular imaging of aggressive epithelial solid tumors

Muynck, L.D.A.N. de

PART II

EVALUATION OF NEW TUMOR-TARGETING CONTRAST AGENTS

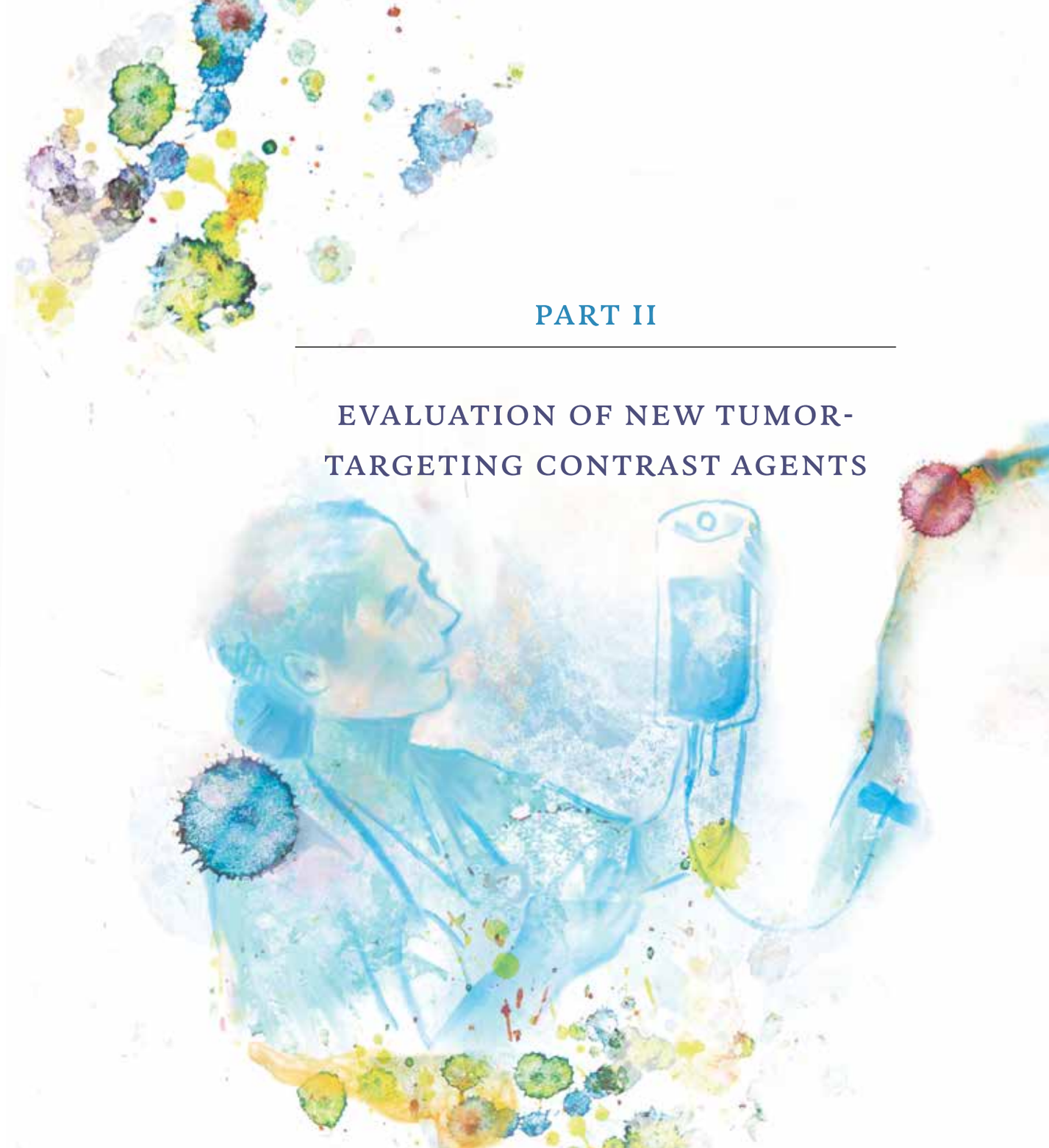

CHAPTER 5

Revolutionizing solid tumor surgery with Fibroblast Activation Protein (FAP)-targeted imaging probes for fluorescence-guided surgery of pancreatic cancer

Bioconjugation. 2025;36(10)

Hanyue Ma[1,2*], **Lysanne D. A. N. de Muynck**[3*], Ruben D. Houvast[3], Savanne Beekman[1,2], Amber Piet[1,2], Taryn L. March[3], Lukas J.A.C. Hawinkels[4], J. Sven D. Mieog[3], Alexander L. Vahrmeijer[3], Yann Seimbille[1,2]
** These authors contributed equally to this work*

1 *Departments of Radiology & Nuclear Medicine; Erasmus MC, Rotterdam, The Netherlands*
2 *Erasmus MC Cancer Institute, Rotterdam, The Netherlands*
3 *Department of Surgery, Leiden University Medical Center, The Netherlands*
4 *Department of Gastroenterology and Hepatology, Leiden University Medical Center, Leiden, The Netherlands*

Abstract

The development of tumor-targeting fluorescent probes to help surgeons detect and remove malignant lesions using near-infrared fluorescence (NIRF)-guided surgery is advancing rapidly. Such advancements show promise for a range of malignancies, expanding the eligibility of patients for surgical intervention and offering improved surgical outcomes. Fibroblast activation protein (FAP), which is present in cancer-associated fibroblasts (CAFs), is overexpressed in the tumor stroma of almost all solid tumors. It is a promising tumor target for NIRF-guided surgery, especially in solid tumors with dense tumor stroma like pancreatic cancer. In this study, we aimed to develop FAP-targeting fluorescent probes with enhanced pharmacokinetics for NIRF-guided surgery of pancreatic cancer. Three novel FAP targeted probes (eFAPs) based on a (4-quinolinoyl)-glycyl-2-cyanopyrrolidine (QCP) structure conjugated to the NIRF dye IRDye800CW were designed and synthesized. All probes displayed excellent inhibition potency and selectivity to FAP. All probes showed specific uptake in FAP-expressing glioblastoma (U87) cells. In *in vivo* optical imaging studies, eFAP-24 exhibited a high mean tumor to background ratio (TBR) of 3.1 ± 0.6 at 24 h post-injection, allowing for clear tumor delineation using the clinical Quest Spectrum NIRF imaging system. Biodistribution analyses showed high fluorescence signal in the tumors and minimal fluorescence signal in all other organs. The successful development and validation of FAP-targeting fluorescent probes, especially eFAP-24, offers promising prospects for enhancing tumor detection and improving surgical outcomes through NIRF-guided surgery, particularly in solid tumors with dense stroma like pancreatic cancer.

Introduction

Pancreatic cancer is a highly lethal disease, often diagnosed at an advanced stage due to its asymptomatic onset.[1] Surgical resection remains the only curative option, yet the majority of patients present with unresectable disease. Despite thorough pre-operative imaging, such as CT scans, up to 80% of tumors are deemed inoperable during exploratory surgery, with occult metastases detected in up to 38% of cases. Achieving negative tumor margins (R0 resection) is crucial for reducing recurrence rates, but remains a significant challenge.[2] Emerging technologies, such as intra-operative near-infrared fluorescence (NIRF) imaging, offer real-time visualization of malignant lesions, facilitating precise delineation of tumor margins and enhancing the likelihood of achieving complete R0 resections. NIRF imaging uses contrast agents with fluorescent characteristics in the NIR region (λ = 700–900 nm), which are visualized by NIR camera systems and displayed on a monitor in real time. Targeted NIRF probes bind specifically to receptors expressed on tumor cells, with minimal binding to healthy tissues, enhancing precision during surgery. This technology holds promise in improving the completeness of resections and ultimately patient outcomes.[3]

Cancer-associated fibroblasts (CAFs) are a key component of the tumor microenvironment (TME) and play a critical role in promoting tumor growth, progression, and metastasis.[4,5] Fibroblast activation protein (FAP), a type II transmembrane glycoprotein expressed on CAFs, is involved in several tumor-promoting processes, including angiogenesis, extracellular matrix remodeling, and immunosuppression. While FAP expression is minimal in healthy tissues, it is significantly upregulated in pathological conditions, particularly in the CAFs of more than 90% of malignant epithelial tumors with dense stromal components,[6] such as pancreatic cancer.[7] In pancreatic cancer, where desmoplasia hinders effective drug delivery to tumor cells, targeting CAFs in addition to tumor cells offers a promising alternative, since CAFs are abundant and more accessible within the stroma.[8,9] The development of tumor-targeting fluorescent probes to help surgeons detect and remove malignant lesions using near-infrared fluorescence (NIRF)-guided surgery is advancing rapidly. Such advancements show promise for a range of malignancies, and better visualization of metastases.

FAP inhibitors exhibiting high binding affinity and specificity to FAP have been extensively studied. FAPI-04 and FAPI-46,[10,11] two of the most

successful small-molecule based inhibitors equipped with metal chelator, have demonstrated high *in vivo* tumor uptake, fast clearance from the circulation and high-contrast PET/CT images in various cancers, including sarcomas and cholangiocarcinoma, and esophageal, breast, lung, hepatocellular, colorectal, head–neck, ovarian, pancreatic, and prostate cancers.[12] [^{68}Ga]FAPI-04 PET/CT demonstrated superior accuracy and sensitivity across primary lesions, metastatic lymph nodes, and distant metastases compared to [^{18}F]-FDG PET/CT in staging pancreatic cancer.[13] Dynamic imaging with [^{68}Ga]FAPI-04 and [^{68}Ga]FAPI-46 showed potential in distinguishing pancreatic cancer from pancreatitis, a challenging differentiation using static imaging alone.[14] These promising results have led to the consideration of FAP as a compelling molecular target for NIRF-guided surgery of pancreatic cancer.

We recently developed a new highly potent FAP ligand, called eFAP, allowing substitutions at the 8-position of the quinoline ring via an ether linkage on the (4-quinolinoyl)-glycyl-2-cyanopyrrolidine (8-QCP) scaffold. eFAP demonstrated high affinity to FAP at a low nanomolar range and has the capacity to be conjugated with various payloads, such as radionuclides, fluorophores, and cytotoxic drugs, for various applications in oncology. For example, in a mouse xenograft model, a DOTA chelator equipped eFAP-6 showed a high and rapid tumor uptake with low background uptake in healthy organs.[15] The high-contrast imaging and rapid clearance, comparable to the clinical reference FAPI-46, suggested that our eFAP ligand is an ideal candidate for tumor-targeted imaging purposes. The encouraging results prompted us to develop new FAP-targeted fluorescent probes based on the eFAP scaffold for NIRF-guided surgery for pancreatic cancer, using IRDye800CW as the NIR dye component. The efficacy of these new probes was subsequently investigated through various *in vitro* and *in vivo* studies.

Materials and Methods

GENERAL METHODS

Chemistry

All chemicals were obtained from commercial suppliers in reagent grade or better and were used without further purification unless specified. All solvents were of analytical or high-performance liquid chromatography (HPLC) grade and used without further purification. Reactions were magnetically stirred and monitored by thin-layer chromatography (TLC) on silica gel 60 F254 aluminum-backed pre-coated plates (Merck; Amsterdam, The Netherlands). Preparative HPLC was conducted using an Agilent 1290 Infinity II Preparative LC System (Middelburg, The Netherlands) equipped with a 1260 Infinity II autosampler, 1260 Infinity II fraction collector, and Agilent 5 Prep C18 column (50 x 21.2 mm, 5 µm), measuring UV absorbance at 230, 254 and 280 nm. The mobile phase consisted of the following: Solvent A, 0.1% formic acid (FA) in water; Solvent B, 0.1% FA in acetonitrile. The default gradient used was 0–8 min, 5–100% B, and 8–10 min, 100% B. The flow rate was 10 ML/min, and chromatograms were recorded using the Agilent OpenLab CDS Chemstation software. Purification of eFAP-17, eFAP-24, eFAP-27 and eFAP-39 was performed using Sep-Pak® C18 cartridges (Waters, Milford, MA, USA). Sep-Pak® C18 cartridges were equilibrated with 5 ML of methanol (MEOH) followed by 10 ML of 5% MEOH in H_2O. Products were eluted using gradient elution of 5 to 95% MEOH in H_2O.

Liquid chromatography-mass spectrometry (LC-MS) was conducted on an Agilent 1260 Infinity II electrospray ionization (ESI) LC-MS system equipped with an Agilent InfinityLab Poroshell 120 EC-C18 column (3.0 x 100 mm, 2.7 µm). Products were eluted using gradient elution of 5 to 100% acetonitrile in H_2O, containing 0.1% FA at a flow rate of 0.5 ML/min for 5 min, monitored at 220, 254, and 280 nm by a UV detector, and at an excitation and emission wavelength of 778 and 794 nm for the fluorescence by a FLD detector. All final compounds showed a single peak at the designated retention time and were at least 95% pure. Melting points (MP) were determined using a Stuart SMP20. NMR spectra were recorded in DMSO-d_6, D_2O or $CDCl_3$ in diluted solutions on a 60 MHZ Nanalysis NMReady 60Pro Calgary, Canada) or a 600 MHZ (Bruker, Billerica, MA, USA) NMR at ambient temperature. Chemical shifts are given as δ values in PPM and coupling constants J are given in HZ. The splitting patterns are reported as S (singlet), D (doublet), T (triplet), Q (quartet), M (multiplet), DD (doublet of doublets), and BR (broad signal). Lyophilization was performed using a FreeZone Benchtop Freeze Dryer (Labconco; Kansas City, MO, USA).

Biology

Molecular Biology Grade Water (Corning; Amsterdam, The Netherlands), referred to here as H_2O, was used in all cases. Recombinant human FAP (h.FAP) (Biolegend; San Diego, CA, USA), recombinant mouse FAP (m.FAP) (Biolegend), recombinant human prolyl oligopeptidase (PREP) protein (R&D Systems;

Minneapolis, MN, USA) and recombinant human dipeptidyl peptidase IV (DPP4) protein (Abcam; Cambridge, UK) were used for enzymatic assays. *In vitro* experiment stock samples were prepared in H_2O and/or DMSO and stored at -20°C. Experiments were performed in 384-well plates (nonbinding, ps, f-bottom, black, high volume) or 96-well plates (black, clear bottom). Plate reader measurements were executed on a Hidex Sense Microplate reader (Hidex; Turku, Finland) at 37°C. Data was collected using the Sense software (Hidex). U87 human glioblastoma cells and U2OS human osteosarcoma cells (ATCC, Manassas, VA, USA) were used for cell uptake experiments. NIR-fluorescence imaging was performed on an Odyssey CLX scanner (Li-Cor; Lincoln, NE, USA). The imaging data were analyzed using Empiria Studio® Software (Li-Cor).

CHEMISTRY SYNTHESIS

Synthesis of 8-QCP-BOC core intermediate

8-QCP-BOC was synthesized through a multi-step organic synthesis procedure (Scheme 1). Detailed information on HPLC, MS and NMR characterizations of intermediates is provided in the Supplementary Materials (Figure S1-S16).

Scheme 1 Chemical synthesis of the BOC-protected 8-QCP (10) core structure. Reagent and conditions: a) NAOH, MEOH, 30 min, rt, 86%; b) i) *N*-hydroxysuccinimide, DCC, RT, 1 h ii) NH_3 in MEOH, RT, 2 h, 72%; c) TFA, DCM, 90%; d) *N*-(*tert*-butoxycarbonyl)glycine, HBTU, DIPEA, RT, 2 h; e) TFAA, pyridine, THF, -15°C to RT, 3 h, 53%, over two steps; f) TFA, DCM, quantitative; g) 1) *tert*-butyl (2-bromoethyl)carbamate, CS_2CO_3, DMF, RT, overnight; 2) NAOH, MEOH, RT, 30 min, 57%; h) HBTU, DIPEA, DMF, RT, 2 h, 72%.

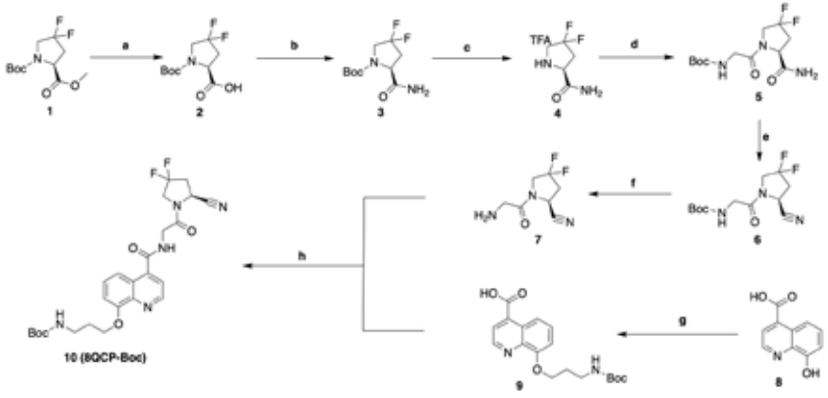

Synthesis of (S)-1-(tert-butoxycarbonyl)-4,4-difluoropyrrolidine-2-carboxylic acid (2)

1-(*Tert*-butyl)-2-methyl(S)-4,4-difluoropyrrolidine-1,2-dicarboxylate (2.06 g, 7.78 mmol) was dissolved in 10 ML MEOH and a solution of sodium hydroxide (0.67 g, 17.18 mmol) in MEOH (15 ML) was added dropwise. The reaction mixture was stirred at room temperature (RT) for 30 min. Upon completion, the reaction mixture was acidified using 1N HCL to PH 2.0 and the aqueous layer was extracted with dichloromethane (DCM) (3 x 50 mL). The combined organic layers were washed with brine, dried using $MGSO_4$ and concentrated *in vacuo*. The product was obtained as an off-white solid (1.62 g, 6.44 MMOL, 86% yield). ^{1}H NMR (60 MHZ, DMSO-d_6) δ 4.33 (DD, *J* = 9.3, 4.4 HZ, 1H), 3.68 (T,*J* = 13.2 HZ, 2H), 2.76 – 2.12 (M, 2H), 1.34 (S, 9H). Mp: 118 – 119°C. ESI-MS *m/z*: calculated for $C_{10}H_{15}F_2NO_4$: 251.10; found: 252.10 $[M+H]^+$.

Synthesis of tert-butyl (S)-2-carbamoyl-4,4-difluoropyrrolidine-1-carboxylate (3)

To a solution of **2** (1.55 g, 6.15 mmol) in dry DCM (30 mL), *N*-hydroxysuccinimide (0.88 g, 7.65 mmol) was added and the mixture was stirred at RT until fully dissolved. *N,N'*-Dicyclohexylcarbodiimide (DCC) (1.55 g, 7.52 mmol) was added to the reaction mixture and stirred at RT for 30 min. A solution of NH_3 in MEOH (4M, 14 mL) was added dropwise and the reaction mixture was stirred at RT for another 3 H. Upon completion, the reaction mixture was diluted by adding ethyl acetate (ETOAC) (50 ML), and the organic layer was washed with saturated aqueous $NAHCO_3$ (5 x 25 ML), brine (25 ML), dried with $MGSO_4$ and concentrated *in vacuo*. The product was obtained as an off-white solid (1.12 g, 4.43 mmol, 72%). ^{1}H NMR (60 MHZ, $CDCL_3$) δ 6.94 – 5.75 (M, 2H), 4.60 – 4.23 (M, 1H), 3.73 (TD, *J* = 12.4, 3.9 HZ, 2H), 2.98 – 2.21 (M, 2H), 1.42 (S, 9H). Mp: 127 – 128°C. ESI-MS *m/z*: calculated for $C_{10}H_{16}F_2N_2O_3$: 250.11; found: 251.11 $[M+H]^+$.

Synthesis of (S)-4,4-difluoropyrrolidine-2-carboxamide (4)

3 (1.0 g, 4.00 mmol) was dissolved in DCM (10 mL) and TFA (5 mL) was added. The reaction mixture was stirred at RT for 2 h. Upon completion, all volatiles were removed under airflow. Cold ether was subsequently added, resulting in the formation of a white solid (0.54 g, 3.60 mmol, 90% yield). The crude product (**3**) was used without further purification. ^{1}H NMR (60 MHZ, DMSO-d_6) δ 9.83 (S, 1H), 8.00 (S, 1H), 7.73 (S, 1H), 4.48 (T, *J* = 8.5 HZ, 1H), 3.71 (t, *J* = 12.4 HZ, 2H), 2.91 (DD, *J* = 12.6, 8.4 HZ, 1H), 2.45 (DD, *J* = 14.7, 8.9 HZ, 1H). Mp: › 130°C. ESI-MS *m/z*: calculated for $C_5H_8F_2N_2O$: 150.06; found: 151.06 $[M+H]^+$.

Synthesis of tert-butyl (S)-(2-(2-cyano-4,4-difluoropyrrolidin-1-yl)-2-oxoethyl)carbamate (6)

4 (0.54 g, 3.60 mmol) was dissolved in DMF (30 mL) and *N*-(*tert*-butoxycarbonyl)glycine (0.76 g, 4.32 mmol), *O*-(benzotriazol-1-yl)-*N,N,N',N'*-tetramethyluronium hexafluorophosphate (HBTU) (1.64 g, 4.32 mmol) and *N,N*-diisopropylethylamine (DIPEA) (3 mL, 2.3 g, 17.6 mmol) were added. The reaction mixture was stirred overnight. Upon completion, ETOAC (50 mL) was added, and the organic layer was washed with brine (5 x 25 mL), dried over $MgSO_4$, and concentrated *in vacuo*. The crude product (**5**) was used for the next step without further purification. **5** was redissolved in tetrahydrofuran (THF) (30 mL) and cooled to -15°C. To the reaction mixture, pyridine (1.00 mL, 0.98 g, 12.4 mmol) and trifluoroacetic anhydride (TFAA) (1 mL, 1.51 g, 7.19 mmol) were added. The reaction mixture was stirred for 3 H, allowed to reach rt. ETOAC (50 mL) and H_2O (50 mL) were added, the layers were separated, and the aqueous layer was extracted with ETOAC (3 x 25 mL). The combined organic layers were washed with H_2O and brine, dried using $MgSO_4$ and concentrated *in vacuo*. The product was purified by flash chromatography (silica gel mesh 40-63 nm, hexane/ETOAC 1:1). The product was obtained as a yellow solid (0.55 g, 1.91 mmol, 53% yield over two steps). ^{1}H NMR (60 MHZ, $CDCl_3$) δ 5.45 (T, *J* = 5.4 HZ, 1H), 4.94 (T, *J* = 6.5 HZ, 1H), 4.14 – 3.61 (M, 4H), 3.02 – 2.34 (M, 2H), 1.40 (S, 9H). Mp: 128 – 129°C. ESI-MS *m/z*: calculated for $C_{12}H_{17}F_2N_3O_3$: 289.12; found: 289.21 $[M+H]^+$.

Synthesis of 8-(3-((tert-butoxycarbonyl)amino)propoxy)quinoline-4-carboxylic acid (9)

8-Hydroxyquinoline-4-carboxylic acid (0.25 g, 1.32 mmol) was dissolved in DMF (25 mL) and 3-(Boc-amino)-propylbromide (0.94 g, 4.0 mmol) and CS_2CO_3 (1.31 g, 4.0 mmol) were added. The reaction mixture was stirred at RT for 2 H. Upon completion, ETOAC (50 mL) was added, and the organic layer was washed with brine (5 x 25 mL), dried using $MgSO_4$ and concentrated *in vacuo*. The residue was redissolved in MEOH (10 mL) and NAOH (78 mg, 2.0 mmol) was added. The reaction mixture was stirred at RT for 35 min. Upon completion, the reaction mixture was concentrated *in vacuo* and the product was purified using HPLC, yielding **9** as a light-yellow solid (0.26 g, 0.75 mmol, 57%). ^{1}H NMR (60 MHZ, DMSO-d_6) δ 8.94 (D, *J* = 4.2 HZ, 1H), 8.16 (D, *J* = 8.3 HZ, 1H), 7.88 (d, *J* = 4.3 HZ, 1H), 7.55 (T, *J* = 8.1 HZ, 1H), 7.18 (D, *J* = 7.4 HZ, 1H), 4.16 (T, *J* = 5.9 HZ, 2H), 3.39 – 2.91 (M, 2H), 1.93 (T, *J* = 6.1 HZ, 2H), 1.32 (S, 9H). MP: > 130°C. ESI-MS *m/z*: calculated for $C_{18}H_{22}N_2O_5$: 346.15; found: 346.72 $[M+H]^+$.

Synthesis of tert-butyl (S)-(3-((4-((2-(2-cyano-4,4-difluoropyrrolidin-1-yl)-2 oxoethyl)carbamoyl)quinolin-8-yl)oxy)propyl)carbamate (10)

6 (0.18 g, 0.61 mmol) was dissolved in DCM (3 mL) and TFA (3 mL). The reaction mixture was stirred at room temperature for 45 min and all volatiles were removed under an air flow. The crude product (7) was used directly without further purification. 7 was redissolved in DMF (5 mL) and **9** (0.2 g, 0.58 mmol), HBTU (0.34 g, 0.87 mmol) and DIPEA (0.35 mL) were added. The reaction mixture was stirred at RT overnight. Upon completion, ETOAC (50 mL) was added, and the organic layer was washed with brine (5 x 25 mL), dried over $MgSO_4$, and concentrated *in vacuo*. The product was purified using flash chromatography (silica gel mesh 40 – 63 nm, hexane/ETOAC 1:1). The product was obtained as a light-yellow solid (0.23 g, 0.44 mmol, 72% yield over 2 steps). ^{1}H NMR (600 MHZ, $CDCl_3$) δ 8.83 (D, *J* = 4.4 HZ, 1H), 7.71 (D, *J* = 8.6 HZ, 1H), 7.51 – 7.35 (M, 2H), 7.25 (T, *J* = 5.1 HZ, 1H), 6.98 (D, *J* = 7.7 HZ, 1H), 6.24 (S, 1H), 4.88 (DD, *J* = 9.0, 3.9 HZ, 1H), 4.30 – 4.14 (M, 2H), 4.10 (DD, *J* = 17.4, 4.7 HZ, 1H), 3.98 – 3.81 (M, 2H), 3.32 (D, *J* = 7.2 HZ, 2H), 2.80 – 2.60 (M, 2H), 2.02 (p, *J* = 5.8 HZ, 2H), 1.38 (S, 9H), 1.20 – 1.11 (M, 1H). ^{13}C NMR (600 MHZ, $CDCl_3$) δ 167.5, 167.4, 156.5, 154.2, 148.2, 141.4, 140.0, 128.4, 126.9, 125.5, 125.3, 123.6, 119.6, 117.1, 116.2, 110.0, 78.9, 68.5, 52.3, 52.0, 51.8, 44.3, 44.3, 42.2, 41.7, 38.9, 37.5, 37.3, 37.1, 29.7, 29.3, 28.6, 19.6. ESI-MS *m/z*: calculated for $C_{25}H_{29}F_2N_5O$: 517.21; found: 517.30 $[M+H]^+$.

SYNTHESIS OF IRDYE800CW EQUIPPED PROBES: EFAP-17, EFAP-24, AND EFAP-27 (*SCHEME 2*)

Synthesis of 8-(3-(4-amino-3-hydroxybutanamido)propoxy)-N-(2-((S)-2-cyano-4,4-difluoropyrrolidin-1-yl)-2-oxoethyl)quinoline-4-carboxamide (13)

To a solution of **10** (20.0 mg, 0.039 mmol) in DCM (1 mL), TFA (1 mL) and triisopropyl silane (TIPS) (20 µL, 10% v/v) were added. After stirring at RT for 30 min, solvents were removed by azeotropic distillation with toluene (3 x 5 mL), giving **11** as a yellow oil. The crude product (**11**) was used in subsequent reactions without further purification. Analytical HPLC retention time: R_t = 3.464 min; ESI-MS *m/z*: calculated for $C_{20}H_{21}F_2N_5O_3$: 417.42; found: 418.10$[M+H]^+$. To a solution of **11** (10.0 mg, 0.024 mmol) in DMF was added 4-((*tert*-butoxycarbonyl)amino)-3-hydrobutanoic acid (7.6 mg, 0.034 mmol), HBTU (20.4 mg, 0.054 mmol), and DIPEA (16.7 µL, 0.096 mmol). After stirring for 1 hour, the reaction mixture was diluted in ETOAC (20 mL), and subsequently washed with H_2O (1 x 10 mL) and brine (2 x 10 mL). The organic layer was dried over $MgSO_4$, filtered, and concentrated *in vacuo* to yield an orange-yellow crude

product. The compound was dissolved in a mixture of DCM (1 mL), TFA (1 mL) and TIPS (50 µl). After stirring 30 min, all solvents were removed under an airstream, and the compound was purified using HPLC to yield **13**, as a yellow solid (10.0 mg, 0.019 mmol, 80%, over two steps). Analytical HPLC retention time: R_t = 3.331 min. ^{1}H NMR (600 MHz, D_2O) δ 9.17 (d, *J* = 5.5 Hz, 1H), 8.22 (d, *J* = 5.5 Hz, 1H), 8.14 – 7.84 (m, 2H), 7.64 (d, *J* = 7.9 Hz, 1H), 4.49 – 4.42 (m, 4H), 4.31 (dd, *J* = 14.2, 11.8, 6.6 Hz, 1H), 4.28 – 4.15 (m, 2H), 3.54 – 3.50 (m, 2H), 3.17 (dd, *J* = 13.2, 3.0 Hz, 1H), 2.98 (dd, *J* = 13.1, 9.8 Hz, 2H), 2.52 (dd, *J* = 14.6, 4.4 Hz, 1H), 2.45 (dd, *J* = 14.6, 8.6 Hz, 1H), 2.21 (t, *J* = 6.4 Hz, 2H). ^{13}C NMR (151 MHz, D_2O) δ 172.4, 168.9, 167.5, 163.0, 162.8, 149.7, 149.1, 143.6, 131.8, 130.4, 126.5, 120.4, 117.3, 116.9, 114.1, 67.3, 64.9, 51.7, 51.5, 44.8, 44.1, 42.2, 40.8, 36.4, 36.2, 27.8. ESI-MS *m/z*: calculated for $C_{24}H_{28}F_2N_6O_5$: 518.52; found: 519.20 $[M+H]^+$.

Scheme 2 Chemical synthesis of the NIRF probes EFAP-17, EFAP-24, and EFAP-27. Reagents and conditions: a) TFA, TIPS, DCM, RT, 30 min; b) 800CW-NHS, DIPEA, DMF, RT, dark conditions, 45 min, 85%; c) i) 4-((*tert*-butoxycarbonyl)amino)-3-hydrobutanoic acid, HBTU, DIPEA, DMF, RT, 1 h; ii) TFA, TIPS, DCM, RT, 30 min, 80% over two steps; d) 800CW-NHS, DIPEA, DMF, RT, dark conditions, 45 min, 79%; e) i) 4-((*tert*-butoxycarbonyl)amino)-3-hydrobutanoic acid, HBTU, DIPEA, DMF, RT, 1 h; ii) TFA, TIPS, DCM, RT, 30 min, 41%, over two steps; f) 800CW-NHS, DIPEA, DMF, rt, dark conditions, 45 min, 72%.

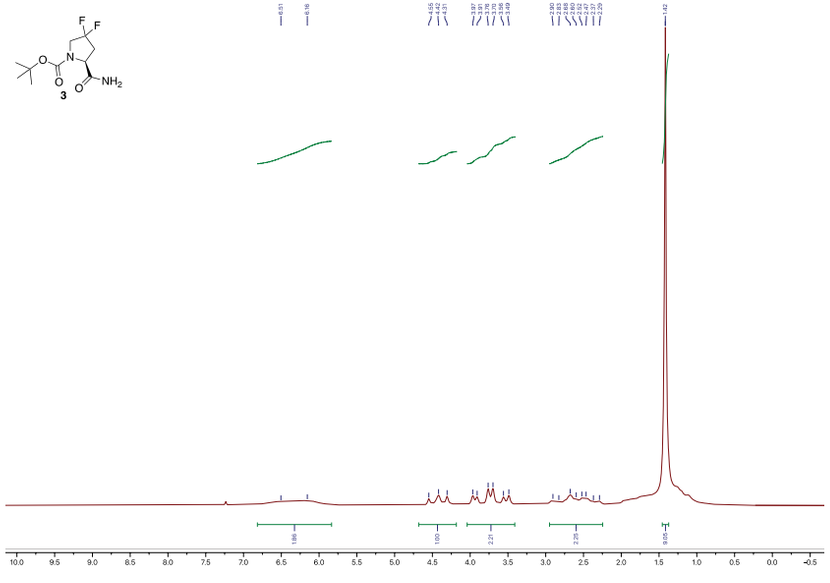

Synthesis of 8-(3-(4-(4-amino-3-hydroxybutanamido)-3-hydroxybutanamido)propoxy)-N-(2-((S)-2-cyano-4,4-difluoropyrrolidin-1-yl)-2-oxoethyl)quinoline-4-carboxamide (15)

To a solution of amine **13** (10 mg, 0.012 mmol) in DMF (2 mL), 4-((*tert*-butoxycarbonyl)amino)-3-hydrobutanoic acid (4.6 mg, 0.021 mmol, 1.1 eq.), HBTU (14.4 mg, 0.038 mmol, 2 eq.), and DIPEA (13.2 µL, 0.076, 4 eq.) were added. After stirring at RT for 1 hour, the reaction mixture was diluted in ETOAC (20 mL), and subsequently washed with H_2O (1 x 10 mL) and brine (2 x 10 mL). The organic layer was dried over $MgSO_4$, filtered, and concentrated *in vacuo* to yield an orange-yellow solid. To the crude product was added a 1:1 mixture of TFA/DCM containing 10% TIPS (1.5 mL), after which the reaction mixture was left to stir at RT for 30 min. Following completion, the reaction mixture was concentrated under an airstream and purified using HPLC to yield **15**, as a yellow solid (4.8 mg, 0.008 mmol, 41% over two steps). Analytical HPLC retention time: R_t = 3.294 min. ^{1}H NMR (600 MHz, D_2O) δ 9.20 – 9.15 (m, 1H), 8.23 (dt, *J* = 7.3, 3.7 Hz, 1H), 8.04 – 7.93 (m, 2H), 7.68 – 7.63 (m, 1H), 5.21 (dq, *J* = 7.9, 3.8 Hz, 1H), 4.50 – 4.42 (m, 4H), 4.35 – 4.24 (m, 1H), 4.20 (tdd, *J* = 14.2, 10.5, 3.4 Hz, 1H), 4.08 (ddq, *J* = 10.5, 6.4, 3.3 Hz, 1H), 3.52 (h, *J* = 3.1 Hz, 2H), 3.38 – 3.15 (m, 4H), 2.99 (tdd, *J* = 10.4, 7.7, 3.1 Hz, 1H), 2.90 (q, *J* = 3.6 Hz, 1H), 2.61 – 2.41 (m, 2H), 2.36 (ddd, *J* = 14.4, 9.0, 3.6 Hz, 1H), 2.21 (q, *J* = 5.6 Hz, 2H), 2.11 – 1.98 (m, 1H). ^{13}C NMR (151 MHz, D_2O) δ 173.3, 172.5, 168.9, 167.5, 163.1, 149.8, 149.0, 143.5, 131.8, 130.3, 126.5, 120.4, 117.3, 117.3, 116.9, 115.4, 114.2, 67.3, 67.2, 67.1, 64.9, 54.9, 51.7, 44.8, 44.6, 44.0, 42.7, 42.2, 40.9, 40.8, 36.6, 36.4, 36.2, 36.1, 27.8. ESI-MS *m/z*: calculated for $C_{28}H_{35}F_2N_7O_7$: 619.63; found: 620.60 $[M+H]^+$.

Synthesis of 4-(2-((E)-2-((E)-3-(2-((E)-1-(6-((3-((4-((2-((S)-2-cyano-4,4-difluoropyrrolidin-1-yl)-2-oxoethyl)carbamoyl)quinolin-8-yl)oxy)propyl)amino)-6-oxohexyl)-3,3-dimethyl-5-sulfoindolin-2-ylidene)ethylidene)-2-(4-sulfophenoxy)cyclohex-1-en-1-yl)vinyl)-3,3-dimethyl-5-sulfo-3H-indol-1-ium-1-yl)butane-1-sulfonate (12, EFAP-17)

To amine **11** (1.6 mg, 3.90 µmol), a solution of IRDye800CW-NHS (5.0 mg, 4.29 µmol) in DMF (1.5 mL) and DIPEA (4.3 µL, 21.45 µmol) was added. The reaction mixture was left to stir at RT for 45 min in the dark, then concentrated *in vacuo* and purified using a Waters Sep-Pak C18 cartridge. The purified fractions were combined and lyophilized, yielding compound **12** (eFAP-17), as a dark green powder (4.7 mg, 3.32 µmol, 85%). ESI-MS *m/z*: calculated for $C_{66}H_{73}F_2N_7O_{17}S_4$: 1402.58; found: 1403.00 $[M+H]^+$. Purity: 97%.

Synthesis of 4-(2-((E)-2-((E)-3-(2-((E)-1-(6-((4-((3-((4-((2-((S)-2-cyano-4,4-difluoropyrrolidin-1-yl)-2-oxoethyl)carbamoyl)quinolin-8-yl)oxy)propyl)amino)-2-hydroxy-4-oxobutyl)amino)-6-oxohexyl)-3,3-dimethyl-5-sulfoindolin-2-ylidene)ethylidene)-2-(4-sulfophenoxy)cyclohex-1-en-1-yl)vinyl)-3,3-dimethyl-5-sulfo-3H-indol-1-ium-1-yl)butane-1-sulfonate (14, EFAP-27)

To compound **13** (2.0 mg, 3.90 µmol), a solution of IRDye800CW-NHS (5.0 mg, 4.29 µmol) in DMF (1.5 mL) and DIPEA (4.3 µL, 21.45 µmol) was added, after which the reaction mixture was stirred in the dark at RT for 45 min. The reaction mixture was concentrated *in vacuo* and purified by Sep-Pak C18 column. The purified fractions were combined and lyophilized, giving **14** (eFAP-27), as a dark green powder (4.3 mg, 3.08 µmol, 79%). ESI-MS *m/z*: calculated for $C_{70}H_{80}F_2N_8O_{19}S_4$: 1503.68; found: 1504.40 $[M+H]^+$. Purity: 98%.

Synthesis 4-(2-((E)-2-((E)-3-(2-((E)-1-(6-((4-((4-((3-((4-((2-((S)-2-cyano-4,4-difluoropyrrolidin-1-yl)-2-oxoethyl)carbamoyl)quinolin-8-yl)oxy)propyl)amino)-2-hydroxy-4-oxobutyl)amino)-2-hydroxy-4-oxobutyl)amino)-6-oxohexyl)-3,3-dimethyl-5-sulfoindolin-2-ylidene)ethylidene)-2-(4-sulfophenoxy)cyclohex-1-en-1-yl)vinyl)-3,3-dimethyl-5-sulfo-3H-indol-1-ium-1-yl)butane-1-sulfonate (16, EFAP-24)

A solution of IRDye800CW-NHS (5.0 mg, 4.29 µmol) in DMF (1.5 mL) and DIPEA (4.3 µL, 21.45 µmol) was added to compound **15** (2.4 mg, 3.90 µmol), after which the reaction mixture was stirred at RT in the dark for 45 min. After evaporation of the solvent under vacuum, the product was purified by Sep-Pak C18 column. The purified fractions were combined and lyophilized, yielding **16** (eFAP-24), as a dark green powder (4.5 mg, 2.81 µmol, 72%). ESI-MS *m/z*: calculated for $C_{74}H_{87}F_2N_9O_{21}S_4$: 1604.79; found: 1605.40 $[M+H]^+$. Purity: 96%.

SYNTHESIS OF THE NEGATIVE CONTROL: (EFAP-39, *SCHEME 3*)

Synthesis of methyl (8-(3-((tert-butoxycarbonyl)amino)propoxy)quinoline-4-carbonyl)glycinate (17)

To a solution of **9** (8.0 mg, 0.023 mmol) in DMF (2 mL), methyl glycinate (4.6 mg, 0.028 mmol), HBTU (17.4 mg, 0.046 mmol), and DIPEA (15.8 µL, 0.092 mmol) were added. After stirring at RT for 1 hour, the reaction mixture was diluted in ETOAC (20 mL), and subsequently washed with H_2O (1 x 10 mL) and brine (2 x 10 ML). The organic layer was dried over $MgSO_4$, filtered, and concentrated *in vacuo* to yield **17**, as an orange-yellow solid (5.2 mg). **17** was used for the next step without further purification. Analytical HPLC retention time: R_t = 4.551 min; ESI-MS *m/z*: calculated for $C_{21}H_{27}N_3O_6$: 417.46; found: 418.11 $[M+H]^+$.

Scheme 3 Chemical synthesis of the negative control EFAP-39. Chemical synthesis of the negative control EFAP-39. Reagents and conditions: a) methyl glycinate, HBTU, DIPEA, DMF, rt, 30 min; b) I) TFA, TIPS, DCM, RT, 30 min; II) NaOH, MEOH, 30 min, 30% over three steps; c) 800CW-NHS, DIPEA, DMF, RT, dark conditions, 45 min, 69%.

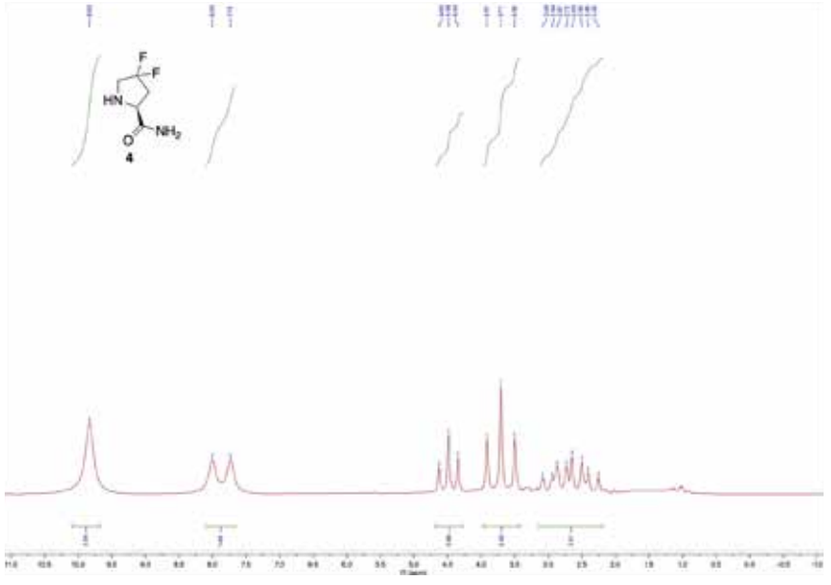

Synthesis of (8-(3-aminopropoxy)quinoline-4-carbonyl)glycine (18)

A 1:1 mixture of TFA/DCM containing 10% TIPS (1.5 mL) was added to **17** (5.2 mg), after which the reaction mixture was left to stir at RT for 30 min. The reaction mixture was concentrated under an airstream, followed by treatment with a solution of NAOH (1.8 mg, 0.046 mmol) in MEOH (2 mL). The reaction mixture was stirred at RT for 30 min. Upon completion, the reaction mixture was neutralized using 1 N HCL, followed by removal of the solvent and purification using HPLC to give compound **18**, as a light-yellow solid (2.1 mg, 6.9 µmol, 30%, over three steps). Analytical HPLC retention time: R_t = 2.709 min;

^{1}H NMR (60 MHz): δ 3.27-3.58 (1H, T), 4.23-4.54 (1H, T), 4.64-4.85 (1H, T), 6.47-6.71 (2H, T), 9.43-10.40 (4H, M), 10.64-11.07 (2H, M). ESI-MS *m/z*: calculated for $C_{15}H_{17}N_3O_3$: 303.32; found: 304.12 $[M+H]^+$.

Synthesis of 4-(2-((E)-2-((E)-3-(2-((E)-1-(6-((3-((4-((carboxymethyl)carbamoyl)quinolin-8-yl)oxy)propyl)amino)-6-oxohexyl)-3,3-dimethyl-5-sulfoindolin-2-ylidene)ethylidene)-2-(4-sulfophenoxy)cyclohex-1-en-1-yl)vinyl)-3,3-dimethyl-5-sulfo-3H-indol-1-ium-1-yl)butane-1-sulfonate (19, EFAP-39)

To compound **18** (1.2 mg, 3.90 µmol), a solution of IRDye800CW-NHS (5.0 mg, 4.29 µmol) in DMF (1.5 mL) and DIPEA (4.3 µL, 21.45 µmol) was added, after which the reaction mixture was left to stir at RT in the dark for 45 min. The reaction mixture was concentrated *in vacuo* and purified using a Sep-Pak C18 column. The purified fractions were combined and lyophilized, yielding compound **19** (eFAP-39), as a dark green powder (3.4 mg, 2.69 µmol, 69%). Analytical HPLC retention time: R_t=3.638 min; ESI-MS *m/z*: calculated for $C_{61}H_{69}N_5O_{18}S_4$: 1288.48; found: 1289.30 $[M+H]^+$. Purity: 95%.

Stability in phosphate-buffered saline (PBS), mouse serum and human serum

Stability studies of 800CW-eFAPs and eFAP-39 were performed by incubation of the compound (50 µL, 10^{-4} M) in PBS (450 µL) at 37°C for up to 24 h. A sample of the PBS solution was directly injected onto the LC-MS at 1, 4 and 24 h post-incubation. Additionally, compounds (50 µL, 10^{-4} M) were incubated with 450 µL of mouse serum or human serum at 37°C for up to 24 h. Following 1, 4, and 24 h of incubation, 50 µL of the serum incubation solution was mixed with 50 µL of acetonitrile in an Eppendorf tube, followed by centrifugation at 5000× *g* for 20 min. The supernatant was analyzed by LC-MS.

DETERMINATION OF LOGD7.4 VALUES

The distribution coefficients ($LogD_{7.4}$) were determined using a shake-flask method, in which 30 µL (10^{-3} M) 800CW-eFAPs were added to an Eppendorf tube containing 1 mL of PBS (0.01 M, PH 7.4)/*n*-octanol (*v*/*v*, 1:1). After vigorous vortexing, the solution was centrifuged at 2500× *g* for 15 min for phase separation. Samples (3 × 50 µL) of the octanol and aqueous phase were taken out and analyzed by LC-MS. $LogD_{7.4}$ values were calculated by using the following equation: $LogD_{7.4}$ = log [(area in octanol phase)/(area in aqueous phase)] and the experiment was performed in triplicate.

IN VITRO INHIBITION STUDIES

All enzymatic assays were performed on black 384-well plates, and enzymatic activity was measured on a microplate reader, monitoring the fluorescence at an excitation and emission wavelength of 355 and 485 nM, respectively. For h.FAP and m.FAP, the reaction mixture comprised substrate (Z-GLY-PRO-AMC, 10 µM), protein (10 ng), assay buffer (50 mM Tris, 100 mM NACL, and 1.5 µM BSA, PH 7.4), and serial dilution of probes from 10^{-5} M to 10^{-11} M to a total volume of 50 µL (1% DMSO, v/v). All components were kept on ice before plating. Val-boroPro (10^{-4} M) and assay buffer (1% DMSO, v/v) served as a positive and negative control, respectively. Plates were incubated at 37°C in the dark for 1 hour. For the PREP assay, the reaction mixture contained substrate (Z-GLY-PRO-AMC, 1 µM), PREP (10 ng), and the same assay buffer as for the FAP assay, with probes serially diluted from 10^{-4} M to 10^{-10} M to a total volume of 50 µL (1% v/v DMSO). The DPP4 assay utilized H-Gly-Pro-AMC (100 µM) as substrate, with DPP4 (0.5 nM) in an assay buffer of 50 mM Tris, 100 mM NACL, PH 8. Probes of interest were serially diluted from 10^{-4} M to 10^{-10} M, maintaining a total volume of 50 µL (1% v/v DMSO). Plates were incubated at 37°C in the dark for 15 min (PREP) or 30 min (DPP4). Val-boroPro (10^{-4} M) and sitagliptin (10^{-4} M) served as a positive control for PREP and DPP4 assay, respectively, while assay buffer was used as a negative control. All experiments were performed in triplicate and repeated three times.

CELL LINES AND CULTURE FOR *IN VITRO* UPTAKE EXPERIMENTS

U87 cells and U2OS cells were used for the cell-based fluorescent uptake experiment, as FAP positive and FAP negative cells, respectively. Cells were cultured in Gibco™ Dulbecco's Modified Eagle Medium (DMEM) (Paisley, UK) supplemented with 2 mM L-glutamine, 10% fetal bovine serum (FBS), 50 units/mL penicillin, and 50 µg/mL streptomycin (Sigma Aldrich, Amsterdam, The Netherlands). Cell lines were passaged twice weekly in tissue culture flasks using trypsin/ethylenediaminetetraacetic acid (trypsin/EDTA) (0.05%/0.02% w/v) and were incubated at 37°C in a 5% CO_2 humidified chamber.

CELL UPTAKE EXPERIMENTS

For *in vitro* uptake studies, all tested compounds were prepared in 5% DMSO solution to prevent stickiness. U87 cells were detached using 0.05% trypsin (Corning; Amsterdam, The Netherlands), re-suspended in 1 million cell aliquots in the binding buffer (1× PBS with 2 mM EDTA and 0.5% FBS) in a 2 mL

centrifuge tube. Cells were incubated with tested compounds at serial dilutions (20, 10, 5, 2.5, 1, 0.5, and 0 nM) for 1 hour at 37°C in a 5% CO_2 humidified chamber. FAP negative U2OS cells were detached, resuspended, and incubated with tested compound (20 nM) following the same procedure and used as a negative control. Cells were treated for 1 hour with IRDye800CW at various concentrations (0 – 20 nM) to determine if the binding of eFAPs was attributable to their specificity to FAP rather than non-specific binding of the dye. Then, cells were washed thrice with ice cold PBS (1 mL, 5% DMSO). Cells were re-suspended in the binding buffer and transferred to a 96-well plate (2 x 10^5 cells/well). NIR-fluorescence imaging was performed on an Odyssey flatbed scanner using the 800 nM channel. Images were collected using Empiria Studio® Software, and the fluorescence intensity was corrected for the background signal.[16]

IN VIVO IMAGING

Patient-derived organoids for in vivo use

Organoid cultures were established from human pancreatic cancer tissue obtained during surgical resection in accordance with the Code of Conduct for Responsible Use of Human Tissues, after written informed consent was obtained from the patients. Organoid cultures were established and cultured as previously described.[17] This study was approved by the medical ethics Committee of Leiden University Medical Center (RP24.004). HPS1 cells were a kind gift of Dr. Regan Koch (Queen Mary Hospital, London, UK).

In vivo fluorescence imaging

The local animal welfare body of the LUMC reviewed and approved all animal studies. Animals were humanely cared for in accordance with the Code of Practice Animal Experiments in Cancer Research and guidelines from Directive 2010/63/EU of the European Parliament on the protection of animals used for scientific purposes. Local standard operating procedures were followed for handling of animals. Six – to twelve-week-old female NSG (NOD.CG-*Prkdcscid Il2rgtm1Wjl/*SZJ) mice were bred in-house and kept at the Central Animal Facility at LUMC and housed per EU Recommendation of 2007-526-EC under specific pathogen-free conditions. Mice were subcutaneously injected with a combination of 250,000 organoid cells (1 well), mixed with $2*10^6$ HPS1 cells (1:8 ratio, reflecting CAF/tumor cell ratios in human PDAC) in Matrigel into the left flank. Tumor growth was monitored with a digital caliper.

Mice bearing subcutaneous tumors of 50 mm^3 were administered with 2 nmol of either eFAP-17, eFAP-24, or eFAP-39 in 100 µl PBS containing Kolliphor (60 µg/mL) and 2% DMSO via tail vein injection (n = 5 per group). Prior to imaging, the tumor and directly adjacent skin were shaved. Fluorescence signal was measured using the clinical Quest Spectrum imaging system (Quest Medical Imaging; Wieringerwerf, The Netherlands). Mice were imaged at 1, 2, 4, 8 and 24 h post-injection (P.I.), and were kept under 2-4% isoflurane anesthesia during imaging. After the final measurement, mice were sacrificed and the tumors and organs were resected and imaged *ex vivo* with the Pearl Trilogy Small Animal imaging system (LI-COR Biosciences; Lincoln, Nebraska USA) to evaluate the biodistribution based on fluorescence signals. Regions of interest (ROIS) were drawn around the tumor and the adjacent background, and tumor-to-background ratios (TBRS) were calculated by dividing the tumor mean fluorescence intensity (MFI) by the background signal. For biodistribution analyses, MFIs were determined by drawing ROIS around the organs. Quest images were analyzed using the Spectrum Capture Suite (Quest Medical Imaging) and MFIs were calculated with ImageJ (version 1.50, National Institutes of Health, Bethesda, MD, USA). Pearl images were analyzed using Image Studio (version 5.2, LI-COR).

HISTOLOGICAL ANALYSIS

Resected tumors were embedded in 4% paraformaldehyde, replaced by ethanol after 24 h, and subsequently embedded in paraffin. Formalin-fixed paraffin-embedded tissue blocks were cut into 4 µm-thick sections. For immunohistochemical staining of FAP, sections were dehydrated in xylene and rehydrated in a stepwise series of alcohol solutions. Endogenous peroxidase activity was blocked with 0.3% hydrogen peroxide for 20 min. FAP epitopes were unmasked by heat induction at 95°C using Tris/EDTA buffer (PH 9.0, Dako, Glostrup, Denmark) in a PT-LINK module (Agilent; Santa Clara, CA, USA). The slides were then incubated overnight in a humidified chamber at RT with a primary rabbit anti-human monoclonal antibody against FAP (1/300, Abcam AB207178). The slides were washed in PBS thrice and incubated for 30 min at RT with a horseradish peroxidase (HRP)-labelled anti-rabbit secondary antibody (Envision, Dako). Slides were rinsed in PBS and immunoreactions were visualized using DAB substrate buffer (Dako) for 10 min and counterstained using Mayer's hematoxylin for 15 s. After dehydration at 37°C, the stained slides were mounted with pertex (Leica Microsystems; Wetzlar,

Germany). Hematoxylin and eosin (H&E) stainings were also made of each FFPE block for histological reference. All stained slides were digitalized using the Panoramic Digital Slide Scanner and viewed with CaseViewer 2.6 (3D Histech; Hungary). For fluorescence imaging, sections were deparaffinized in xylene, left to evaporate for 1-2 h, and coverslipped with EverBrite™ Hardset Mounting Medium with DAPI (Biotium; Fremont, CA, USA) followed by fluorescence imaging using the ZEISS Axio Scan.Z1 (Carl Zeiss). Images were analyzed using Zen Lite (version 3.9, Carl Zeiss).

STATISTICS

Data were presented as mean ± standard deviation (SD) and all statistical analyses were performed with GraphPad Prism version 9.0 (San Diego, California USA). All IC50 values were 22 determined using a non-linear regression Log-(inhibitor) vs. response analysis with variable slope (four-parameters). All *in vitro* experiments were performed in triplicate and repeated three times. For *in vivo* experiments, n = 5 mice per group/time point were imaged, as at least three are needed to calculate standard deviation, with two extra included to account for potential dropout or lack of tumor growth. MFI's were calculated from all five mice per time point, with each measurement taken from distinct mice (no repeated measurements). A two-way ANOVA (two-sided) was used to assess differences in MFI across time points. Sidak's multiple comparisons test was applied to correct for multiple comparisons. Camera settings (exposure time of 100 ms) were kept constants for all measurements to ensure consistency. Figures were created with BioRender.com (full license).

Results

FAP-TARGETED NIRF PROBES AND NEGATIVE CONTROL DESIGN

Fluorescent probes, eFAP-17, eFAP-24 and eFAP-27 incorporated the 8-QCP backbone targeting FAP. All three probes were conjugated to the clinically validated NIRF dye, IRDye800CW. IRDye800CW was directly coupled to the 8-QCP scaffold for eFAP-17, while hydrophilic linkers, based on 4-amino-3-hydroxybutanoic acid (GABOB), were introduced between the 8-QCP moiety and the dye to improve the hydrophilicity of eFAP-24 and eFAP-27. To facilitate a more comprehensive evaluation of these eFAP probes *in vivo*, a negative control eFAP-39 was designed and synthesized. The structure of eFAP-39 closely resembles that of eFAP-17, except for the absence of the cyanopyrrolidine moiety, ensuring similar metabolism and pharmacokinetics.

Figure 1 Chemical structure of IRDYE800CW (green) equipped FAP binding unit (8-QCP) with or without GABOB (red) linker (EFAP-17, EFAP-24, and EFAP-27) and the negative control EFAP-39. The difference between EFAP-17 and EFAP-39 is highlighted in orange.

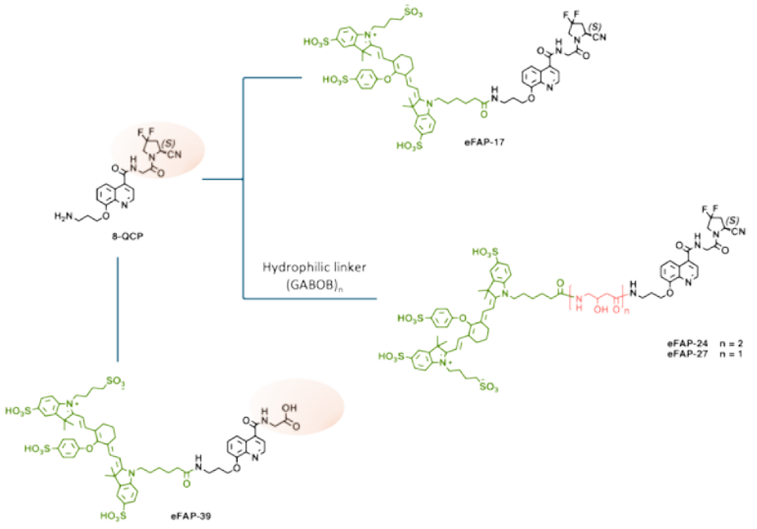

CHEMICAL SYNTHESIS

The syntheses of (4-quinolinoyl)-glycyl-2-cyanopyrrolidine (8-QCP)-based FAP probes are presented in Schemes 1-3. Initially, 1-(*tert*-butyl)-2-methyl(S)-4,4-difluoropyrrolidine-1,2-dicarboxylate was demethylated in the presence of NAOH in MEOH to afford intermediate **2** in 86% yield. Amination of **2** was performed via activation into a NHS ester using *N*-hydroxysuccinimide and DCC in DMF, followed by treatment with an ammonia solution in MEOH, resulting in amide **3** in 72%. Removal of the *tert*-butyloxycarbonyl (Boc) protecting group from **3** was conducted in a TFA/DCM mixture, affording compound **4** in 90% yield. The deprotected **4**, containing a free secondary amine, was ready to be coupled with *N*-(*tert*-butoxycarbonyl)glycine in the presence of HBTU and DIPEA in DMF, affording intermediate **5**. The latter was then treated with trifluoroacetic anhydride and pyridine in THF to obtain the corresponding

nitrile **6** in a 53% yield over two steps. Etherification of 8-hydroxyquinoline-4-carboxylic acid (**8**) was conducted in a two-step procedure using *tert*-butyl (2-bromoethyl)carbamate in the presence of Cs_2CO_3, followed by treatment with NaOH in MeOH, providing **9** in a 57% yield over two steps. Removal of the Boc protecting group from **6** using TFA/DCM (1:1) prior to reacting it with the quinoline **9** afforded the desired intermediate 8-QCP-Boc (**10**) in a yield of 72%.

To obtain the IRDye800CW-conjugated probe eFAP-17, the Boc protecting group was removed from **10** using acidic conditions and the resulting amine **11** subsequently reacted with IRDye800CW-NHS ester, to give **12** (eFAP-17). Next, the core structure of 8-QCP was extended by incorporating GABOB units. This was achieved by reacting **11** with 4-((tert-butoxy carbonyl)amino)-3-hydrobutanoic acid. Repeated Boc deprotection and GABOB coupling led to the preparation of the elongated compounds **13** and **15**, containing one and two GABOB units, respectively. Upon reaction with IRDye800CW-NHS ester, the fluorescent probes 14 (eFAP-27) and **16** (eFAP-24) were successfully synthesized.

To synthesize the negative control **19** (eFAP-39), quinoline **9** was reacted with methyl glycinate to yield **17** followed by deprotection of the Boc and methyl protecting groups. The resulting amine **18** was coupled to IRDye800CW-NHS ester to give **19** (eFAP-39).

STABILITY AND LIPOPHILICITY

The stability of eFAP-17, eFAP-24 and eFAP-27 was analyzed through LC analysis (Table 1, Figure 2) after incubation in PBS, mouse serum (MS) and human serum (HS) (n = 3). Both eFAP-24 and eFAP-27 showed a strong hydrophilic character with $LogD_{7.4}$ values of -2.10 ± 0.31 and -1.62 ± 0.09, respectively. eFAP-17 demonstrated a more lipophilic nature ($LogD_{7.4}$ = -0.95 ± 0.02). The increased hydrophilic properties of eFAP-24 and eFAP-27 could be attributed to the introduction of the GABOB linkers.

Additionally, all three eFAP probes exhibited outstanding stability in PBS for at least 24 h, with less than 3% degradation. Remarkably, eFAP-24 displayed the highest stability, retaining 98.6 ± 1.44%, 97.7 ± 0.76% and 98.5 ± 1.33% of its integrity in PBS, MS, and HS, respectively. eFAP-27 showed a decreased stability compared to eFAP-24 but remained more than 90% intact after 24 h. Although, eFAP-17 was highly stable in PBS (97.5 ± 0.49%, at 24 h), a decrease in integrity was observed over time in MS and HS, resulting in 54.07 ± 5.52% and 82.22 ± 0.53% intact eFAP-17 at 24 h, respectively. The reduced stability of eFAP-17 compared to the other two probes is likely due to its higher lipophilicity, which leads to increased binding to serum proteins, thereby lower the intensity of eFAP-17 signal detected in the LC chromatogram. Moreover, eFAP-39 showed no significant degradation when incubated in PBS, MS, and HS for 24 h.

Table 1 Lipophilicity ($LogD_{7.4}$) and stability studies.

		Stability (%, 24 h)		
	$LogD_{7.4}$	PBS	mouse serum	human serum
eFAP-17	-0.95 ± 0.02	97.5 ± 0.49	54.1 ± 5.52	82.2 ± 0.53
eFAP-24	-2.10 ± 0.31	98.6 ± 1.44	97.7 ± 0.76	98.5 ± 1.33
eFAP-27	-1.62 ± 0.09	97.8 ± 0.01	92.6 ± 2.23	96.6 ± 1.99
eFAP-39	-	97.6 ± 0.40	96.9 ± 1.39	99.0 ± 0.65

Figure 2 Stability studies. (A) Stability of EFAP-17 incubated in PBS after 1 h (99.9 ± 0.06%), 4 h (99.9 ± 0.06%), 24 h (97.5 ± 0.49%); in mouse serum after 1 h (96.4 ± 1.08%), 4 h (70.0 ± 4.54%), 24 h (54.1 ± 5.52%); in human serum after 1 h (99.9 ± 0.17%), 4 h (97.7 ± 0.50%), 24 h (82.2 ± 0.53%). (B) Stability of EFAP-24 incubated in PBS after 1 h (98.6 ± 1.44%), 4 h (99.0 ± 1.54%), 24 h (98.6 ± 1.44%); in mouse serum after 1 h (99.8 ± 0.17%), 4 h (99.0 ± 0.82%), 24 h (97.7 ± 0.76%); in human serum after 1 h (>99.9%), 4 h (98.7 ± 1.42%), 24 h (98.5 ± 1.33%). (C) Stability of EFAP-27 incubated in PBS after 1 h (>99.9%), 4 h (99.9 ± 0.06%), 24 h (97.8 ± 0.01%); in mouse serum after 1 h (98.5 ± 1.26%), 4 h (98.2 ± 0.65%), 24 h (92.6 ± 2.23%); in human serum after 1 h (99.0 ± 1.54%), 4 h (98.6 ± 0.38%), 24 h (96.6 ± 1.99%). (D) Stability of EFAP-39 incubated in PBS after 1 h (99.5 ± 0.89%), 4 h (98.8 ± 1.43%), 24 h (97.6 ± 0.40%); in mouse serum after 1 h (98.4 ± 1.06%), 4 h (99.2 ± 0.29%), 24 h (96.9 ± 1.39%); in human serum after 1 h (99.8 ± 0.17%), 4 h (99.2 ± 0.47%), 24 h (99.0 ± 0.65%). *(figure on next page)*

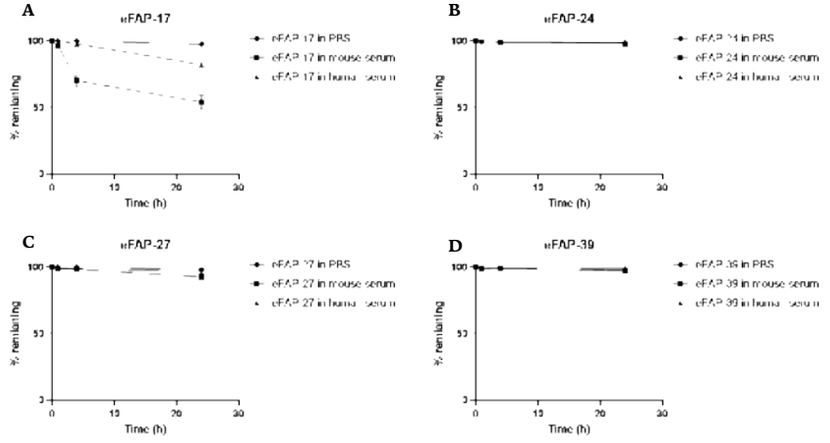

BINDING AFFINITY

The inhibitory potency against human FAP (h.FAP) and murine FAP (m.FAP) proteins were determined in a recombinant enzymatic assay that relies on the cleavage of fluorescent AMC from a Z-GLY-PRO-AMC substrate. All three FAP probes exhibited remarkable binding affinity to both h.FAP and m.FAP, with IC_{50} values in the low nanomolar range (IC_{50}, human FAP < 6 nm, IC_{50}, murine FAP < 5 nm, Figure 3A and 3B, Table 2), comparable to FAPI-46 (IC_{50}, human FAP = 3.87 ± 2.7 nm, IC_{50}, murine FAP = 1.55 ± 1.2 nm). Notably, eFAP-24 displayed the highest inhibitory activity against FAP (eFAP-24: IC_{50}, human FAP = 3.04 ± 0.18 nm, IC_{50}, murine FAP = 2.96 ± 0.15 nm). Additionally, to evaluate the selectivity, enzymatic assays with prolyl oligopeptidase (PREP) and dipeptidyl peptidase IV (DPP4), proteins belonging to the same family as FAP, were conducted. Similar to the FAP enzymatic assays, IC_{50} values for PREP and DPP4 were determined by incubating recombinant human PREP and recombinant human DPP4 with a Z-GLY-PRO-AMC and H-GLY-PRO-AMC substrate, respectively (Table 2, Figure 3C and 3D). All three probes demonstrated affinity for PREP in the µM range (IC_{50} = 0.32-2.00 µM), resulting in high PREP/FAP selectivity indexes (SI) >100. The IC_{50} values of eFAPs against DPP4 were in the low millimolar range, indicating high selectivity in favor of FAP targeting (Table 2). Enzymatic assay of eFAP-39 on both h.FAP and m.FAP confirmed the extremely low binding of eFAP-39 to FAP proteins.

Table 2 IC_{50} values determined by an enzymatic assay and selectivity indexes (SI).

	Inhibition		Selectivity		Selectivity indexes (SI)	
	IC_{50}, human FAP (nm)	IC_{50}, murine FAP (nm)	IC_{50}, PREP (nm)	IC_{50}, DPP4 (nm)	PREP/FAP	DPP4/FAP
FAPI-46	3.87 ± 2.7	1.55 ± 1.2	3480 ± 172.5	20540 ± 2526	899.2	5307.5
eFAP-17	5.65 ± 0.19	5.0 ± 0.2	2000.7 ± 376.8	15170 ± 4200	354	2685
eFAP-24	3.04 ± 0.18	2.96 ± 0.15	322.4 ± 43.8	13587 ± 3970	106	4469
eFAP-27	4.01 ± 0.28	3.72 ± 0.11	667.3 ± 213.7	28100 ± 2667	166	7007
eFAP-39	> 1 mM	> 1 mM	N.D.	N.D.	-	-

N.D.: not determined.

Figure 3 IC_{50} curves of FAPI-46, EFAP-17, EFAP-24, EFAP-27, and EFAP-39 on proteins.
(A) Recombinant human FAP. (B) Recombinant murine FAP. (C) Recombinant PREP. (D) Recombinant DPP4.

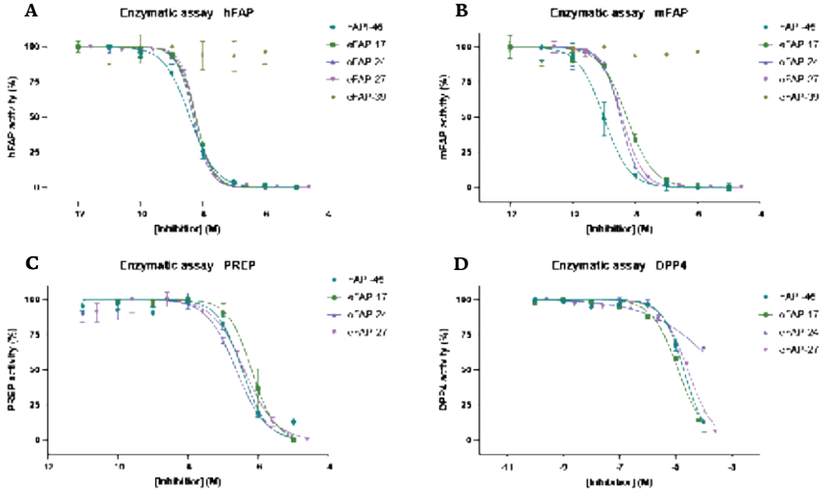

CELL UPTAKE

In vitro uptake studies were conducted on both FAP positive (U87) and FAP negative (U2OS) cell lines (Figure 4). Binding of all three probes to U87 was observed and exhibited concentration-dependent binding. Notably, binding of eFAP-17 and eFAP-27 reached saturation with 10 nm, while eFAP-24 still showed an increasing trend when treated with higher concentration (Figure 4B). Consequently, eFAP-24 exhibited the highest uptake (27.57 ± 2.02% AD) compared to eFAP-17 (3.55 ± 0.42% AD) and eFAP-27 (6.54 ± 0.81% AD) (Figure 4D). A limited non-specific binding of all probes was observed in FAP-negative U2OS cells when incubated with a high concentration (20 nm) of the probes (Figure 4A). Moreover, the negative control eFAP-39 did not show binding to both FAP-positive and FAP-negative cell lines (Figure 4A-D).

Figure 4 Cellular uptake studies on FAP-positive cell line (U87) and FAP-negative cell line (U20S). (A) Cells incubated with various concentrations of EFAPs were imaged to determine binding of the EFAPs on U87 and U20S cells. (B) Dose-response curves of EFAP probes and negative control binding toU87 cells. (C) Fluorescence signal of EFAPs (0.5 – 20 nM) binding to U87 and U20S (-) cells. (D) Fluorescence signal of EFAPs (0.5 – 20 nM) binding to U87 and U20S (-) cells normalized to the added dose.

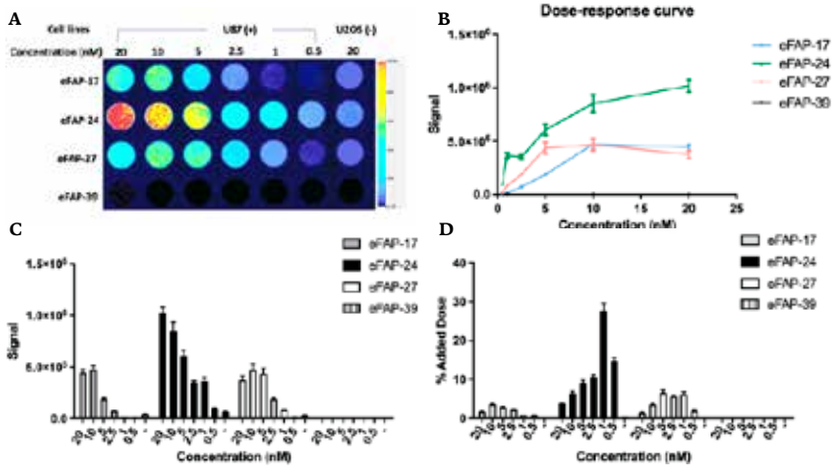

IN VIVO BINDING CHARACTERISTICS

With the highest binding affinity, stability, and superior uptake in FAP-positive cells, eFAP-24 was selected for further *in vivo* evaluation; eFAP-17 and eFAP-27 demonstrated similar uptake, however, to assess the structural variations and the impact of hydrophilic linker introduction, eFAP-17 was chosen as the second probe *in vivo*, despite its slightly reduced stability. eFAP-39 served as a negative control.

A significant difference was observed between the tumor and background fluorescence from 8 to 48 h post injection (P.I.) of eFAP-24 (Figure 5A). However, no such contrast could be visualized in mice administered with eFAP-17 and eFAP-39. The highest TBR (3.1 ± 0.6) was seen with eFAP-24 at 24 h P.I., allowing for clear tumor delineation using the clinical Quest Spectrum imaging system. A lower TBR was observed for eFAP-17 and the negative control eFAP-39 at 24 h P.I. (1.2 ± 0.1 and 0.9 ± 0.1, respectively) (Figure 5B,C). This emphasizes both the pharmacokinetic advantage and improved binding affinity of the more hydrophilic eFAP-24.

Figure 5 *In vivo* fluorescence imaging. (A) MFI's of EFAP-17, EFAP-24 and EFAP-39 of tumor and corresponding background tissue. (B) TBR's of all three probes. (C) *In vivo* fluorescence images at 24h. T; tumor, B; background. White arrows point at tumors.

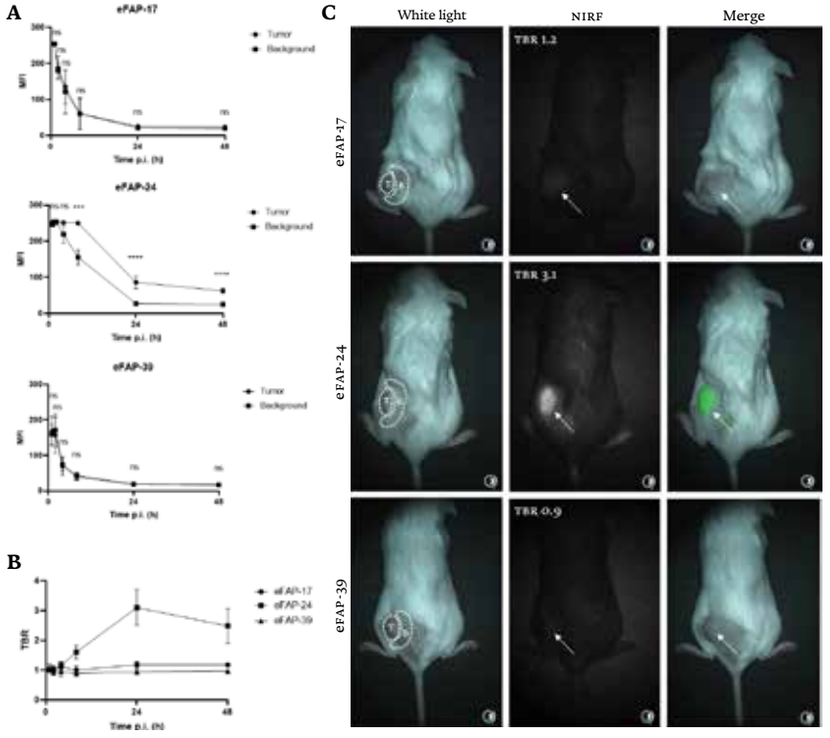

*Abbreviations: NS, not significant, ***p = 0.0001, ****p = <0.0001.*

Biodistribution analyses at 48 h p.i. showed a high fluorescence signal in resected tumors of mice administered with eFAP-24, accompanied by minimal fluorescence in healthy organs (Figure 6A and B). For eFAP-17 and eFAP-39, fluorescence signal in the tumors was lower and was similar to the fluorescence signal in healthy organs. Although, eFAP-24 showed a slightly increased signal in excretory organs, such as the kidneys and the liver compared to healthy tissue (Figure 6A and B), higher tumor/kidneys (T/K) and tumor/liver (T/L) ratios were observed for eFAP-24 (T/K: 3.3, T/L: 5.3) compared to eFAP-17 (T/K: 1.8, T/L: 2.7) and eFAP-39 (T/K: 1.3, T/L: 1.8). Increased signal was also seen in the stomach for all three probes; however, this is a consequence of the presence of chlorophyll-containing alfalfa and its derivatives in mouse food, which is known to fluoresce in the NIR region. Using a clinically relevant stroma-rich, organoid-based *in vivo* model of human PDAC, these findings highlight the superior potential of eFAP-24 as a tracer for FAP-targeted NIRF imaging of pancreatic cancer.

Histological analysis showed that NIRF signals for eFAP-24 overlapped with microscopically identified tumor stroma areas, as well as FAP staining (Figure 6C), thereby confirming binding specificity of the probe, and indicating complete tumor penetration.

Figure 6 ***Ex vivo*** **analysis of EFAP-17, EFAP-24, and EFAP-39.** (A) MFIs of resected organs. (B) Fluorescence images of resected organs taken with the Pearl imaging system. (C) H&E, immunohistochemistry and NIR fluorescence images of resected tumors. Scale bars represent 500 µm. Scale bars in zoomed in fluorescence images represent 50µm. 1: lungs, 2: heart, 3: pancreas, 4: spleen, 5: stomach, 6: duodenum, 7: cecum, 8: rectum, 9: skin, 10: brain, 11: tumors, 12: skin, 13: liver, 14: kidneys.

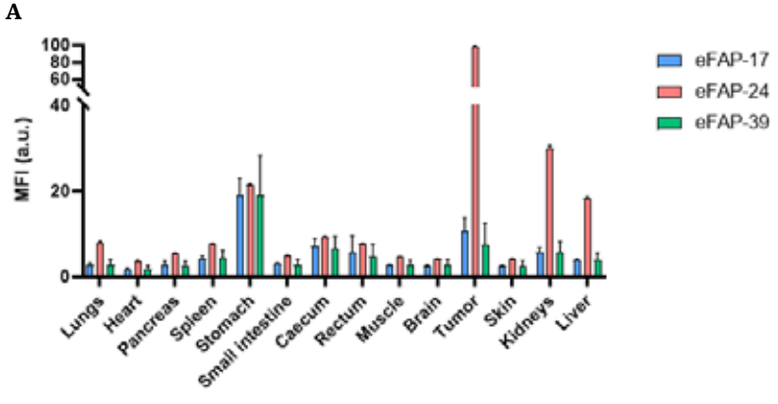

(Continuation Figure 6)

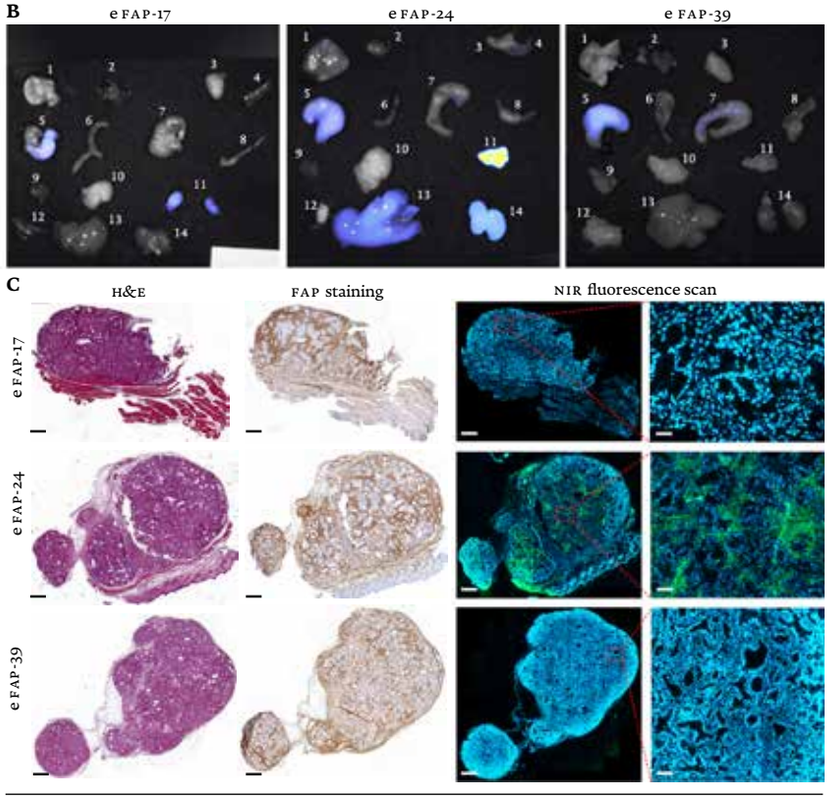

Discussion

NIRF-guided surgery holds great promise for improving radical resection rates by offering surgeons real-time visualization of tumor tissue during operations. However, the ongoing difficult search for targeting molecules with optimal pharmacokinetics remains crucial, particularly in tumors with dense stroma, such as pancreatic cancer. In this study, we developed three novel FAP-targeted fluorescent probes, eFAP-17, eFAP-24, and eFAP-27, conjugated with IRDye800CW dye for NIRF imaging and assessed their effectiveness for real-time FAP-mediated imaging in pancreatic cancer. Of these, eFAP-24 demonstrated high stability, significant *in vitro* uptake, and the ability to

clearly distinguish tumor lesions from surrounding tissue in a clinically relevant PDAC xenograft model, achieving the highest TBR *in vivo*. This study underscores the potential value of FAP-targeted imaging in addressing the unmet need for tools that improve tumor delineation during complex oncologic surgeries.

Targeting tumor cell surface receptors is a traditional approach for NIRF imaging due to their high specificity for cancer cells. However, the challenge lies in the heterogeneity of receptor expression, which can vary between tumors and even within different areas of the same tumor, potentially resulting in incomplete visualization during surgery.[18] In contrast, targeting the tumor stroma offers several advantages, especially in cancers with dense fibrotic tissue, like pancreatic cancer.[19] FAP is abundantly expressed in CAFs in the stromal compartment surrounding the tumor. Due to their high genetic stability and homogeneity, CAFs enable more consistent and widespread targeting across different tumors.[9,20] This approach ensures that even poorly vascularized, hypoxic, or necrotic tumor regions that are difficult to access with cell-targeting agents can still be targeted by NIRF probes. This makes it particularly advantageous for NIRF-guided surgery, especially in challenging surgical environments like pancreatic cancer, where the precision of visualization is even more critical as surgeons can no longer rely on tactile feedback for tumor identification.

Our novel probes featuring the (4-quinolinoyl)-glycyl-2-cyanopyrrolidine backbone as the FAP-binding moiety, were synthesized via a rapid and straightforward procedure. All probes exhibited nanomolar inhibition of both human and murine FAP (IC_{50} < 6 nm), suggesting a limited influence of the modification at the 8-position of QCP on the binding affinity of the eFAP analogs. The introduction of the GABOB linkers enhanced the IC_{50} against FAP, confirming that an increased distance between the dye and QCP is required to preserve the binding affinity. The minor loss of affinity likely results from the bulk structure of the NIRF dye hindering the binding moiety from accessing the binding pocket on FAP. Additionally, similar to FAP, the inclusion of GABOB resulted in better inhibitory activity against PREP, which led to less selectivity of the probes to FAP. Nevertheless, with high PREP/FAP and DPP4/FAP selectivity indexes (SI: PREP/FAP >100, SI: DPP4/FAP >2000), the eFAP probes retained high specificity. The hydrophilic character of GABOB also contributed to improved hydrophilic properties of the fluorescent probes. Moreover, all probes demonstrated high stability in PBS, MS, and HS for up to 4 h, with less than 5% degradation. Among the probes, eFAP-24, which possesses two GABOB units, exhibited the highest inhibitory activity against human FAP and murine FAP (3.04 ± 0.18 nm and 2.96 ± 0.15 nm, respectively) and the highest hydrophilicity ($LogD_{7.4}$ = -2.10 ± 0.31). Remarkably, eFAP-24 displayed the highest stability, retaining > 97% in PBS, MS, and HS after 24 h.

eFAP-24 also stood out among the synthesized probes with its favorable *in vivo* performance. Its ability to clearly delineate tumor lesions from surrounding healthy tissue with a high tumor-to-background ratio (TBR of 3.1) in a clinically relevant tumor model is particularly noteworthy. This is especially important for pancreatic cancer, where the ability to differentiate between tumor and healthy pancreatic tissue is critical for ensuring complete resection while preserving as much healthy tissue as possible. Moreover, by incorporating IRDye800CW, a dye already proven safe in clinical studies,[21–23] we enhance the translational potential of eFAP-24 for clinical use. The use of a targeting molecule with a relatively lower weight will facilitate easier, more cost-effective, and straightforward synthesis, thereby further enhancing the potential for clinical translation. The use of a clinically relevant NIR camera system further strengthens the case for its integration into surgical workflows, enabling real-time imaging of FAP-expressing tumors and potentially improving patient outcomes by guiding more accurate tumor resection. Additionally, by focusing on FAP, a hallmark of desmoplasia, the probe could not only allow for tumor-specific imaging but may also provide insights into the stromal contribution to tumor biology. This dual functionality could have applications beyond surgery, such as in monitoring therapy response, or imaging fibrotic/stenotic lesions in the colon in patients with inflammatory bowel disease.

A limitation of this study is that the expression of FAP in tumor tissues after neoadjuvant therapy was not comprehensively evaluated. Although a previous study from our group investigated the expression of FAP, among other markers, in PDAC tissue after neoadjuvant therapy, it was based on a small cohort and utilized a different antibody.[24] It is important to note that FAP antibodies have demonstrated considerable variation in their effectiveness. Neoadjuvant therapy is increasingly being used to improve survival and R0 resection rates in pancreatic cancer but can significantly reduce target expression.[25,26] If FAP expression is diminished post-therapy, the utility of eFAP probes for intra-operative imaging might be compromised, as

tumors may not be sufficiently visualized during surgery. However, therapies usually target rapidly dividing cells, which is not the case for fibroblasts. Additionally, fibroblasts are known to be more resistant to conventional therapies.[4] Moreover, inflammation and fibrosis/necrosis caused by radio/chemotherapy can lead to increased FAP expression in surrounding tissue, leading to elevated background signals. This heightened background signal complicates the ability to distinguish tumor boundaries from background tissue during surgery. These underscore the importance of future studies to investigate how FAP expression changes in response to neoadjuvant therapy.

Additionally, while eFAP-24 showed favorable *in vitro* and *in vivo* binding characteristics, the highest TBR was observed after 24 h, despite an increase in MFI over time. This is attributed to the presence of the GABOB linker, which increases the retention time of the probe in the tumor. Ideally, we would like to inject a probe just before surgery to avoid requiring the patient to visit the hospital multiple times. However, in this case, it may still be worthwhile to have the patient come in a day earlier, as long as the probe provides a significant benefit for the patient during surgery. A complementary biodistribution study at early time points is necessary to gain insight into the pharmacokinetics of eFAP-24 and better understand the influence of the linker.

Our findings establish eFAP-24 as a groundbreaking candidate for NIRF-guided surgery in pancreatic cancer, demonstrating enhanced tumor specificity, optimized pharmacokinetics, and real-time imaging capabilities that surpass existing probes. This study not only addresses a critical need in pancreatic cancer surgery but also sets a new standard for targeting stromal biomarkers, potentially transforming imaging strategies for various FAP-expressing tumors. The ability of the eFAP-800CW probe to enhance intraoperative visualization of tumor margins is particularly relevant in reducing the incidence of positive resection margins, a key determinant of patient prognosis. Future research will aim to refine eFAP-24 for clinical application, further building its significant potential for improving surgical outcomes and patient management in oncology.

REFERENCES

1. Bengtsson, A., Andersson, R. & Ansari, D. The actual 5-year survivors of pancreatic ductal adenocarcinoma based on real-world data. Sci Rep 10, 16425 (2020).
2. Ethun, C.G. & Kooby, D.A. The importance of surgical margins in pancreatic cancer. Journal of surgical oncology 113, 283-288 (2016).
3. Mieog, J.S.D. et al. Fundamentals and developments in fluorescence-guided cancer surgery. Nature reviews Clinical oncology 19, 9-22 (2022).
4. De, P., Aske, J. & Dey, N. Cancer-associated fibroblast functions as a road-block in cancer therapy. Cancers 13, 5246 (2021).
5. Cirri, P. & Chiarugi, P. Cancer-associated-fibroblasts and tumour cells: a diabolic liaison driving cancer progression. Cancer and Metastasis Reviews 31, 195-208 (2012).
6. Garin-Chesa, P., Old, L.J. & Rettig, W.J. Cell surface glycoprotein of reactive stromal fibroblasts as a potential antibody target in human epithelial cancers. Proceedings of the National Academy of Sciences 87, 7235-7239 (1990).
7. Hessmann, E. et al. Microenvironmental determinants of pancreatic cancer. Physiological reviews (2020).
8. Hingorani, S.R. Epithelial and stromal co-evolution and complicity in pancreatic cancer. Nature Reviews Cancer 23, 57-77 (2023).
9. Norton, J., Foster, D., Chinta, M., Titan, A. & Longaker, M. Pancreatic cancer associated fibroblasts (CAF): under-explored target for pancreatic cancer treatment. Cancers 12, 1347 (2020).
10. Jansen, K. et al. Selective inhibitors of fibroblast activation protein (FAP) with a xanthine scaffold. MedChemComm 5, 1700-1707 (2014).
11. Lindner, T. et al. Development of quinoline-based theranostic ligands for the targeting of fibroblast activation protein. Journal of Nuclear Medicine 59, 1415-1422 (2018).
12. Zhao, L. et al. Fibroblast activation protein-based theranostics in cancer research: A state-of-the-art review. Theranostics 12, 1557-1569 (2022).
13. Ding, J. et al. Comparing the clinical value of baseline [(68) Ga]Ga-FAPI-04 PET/CT and [(18)F]F-FDG PET/CT in pancreatic ductal adenocarcinoma: additional prognostic value of the distal pancreatitis. Eur J Nucl Med Mol Imaging 50, 4036-4050 (2023).
14. Röhrich, M. et al. Impact of 68Ga-FAPI PET/CT imaging on the therapeutic management of primary and recurrent pancreatic ductal adenocarcinomas. Journal of Nuclear Medicine 62, 779-786 (2021).
15. van der Heide, C.D. et al. *In vitro* and *in vivo* analyses of EFAP: a novel FAP-targeting small molecule for radionuclide theranostics and other oncological interventions. EJNMMI Radiopharm Chem 9, 55 (2024).
16. Slania, S.L. et al. Imaging of Fibroblast Activation Protein in Cancer Xenografts Using Novel (4-Quinolinoyl)-glycyl-2-cyanopyrrolidine-Based Small Molecules. Journal of Medicinal Chemistry 64, 4059-4070 (2021).
17. Harryvan, T.J. et al. A Novel Pancreatic Cancer Mini-tumor Model to Study Desmoplasia and Myofibroblastic Cancer-Associated Fibroblast Differentiation. Gastro Hep Adv 1, 678-681 (2022).
18. van Dam, M.A. et al. Overview and Future Perspectives on Tumor-Targeted Positron Emission Tomography and Fluorescence Imaging of Pancreatic Cancer in the Era of Neoadjuvant Therapy. Cancers 13, 6088 (2021).
19. Xu, M., Zhang, T., Xia, R., Wei, Y. & Wei, X. Targeting the tumor stroma for cancer therapy. Mol Cancer 21, 208 (2022).
20. Saude-Conde, R. et al. Cancer-Associated Fibroblasts in Pancreatic Ductal Adenocarcinoma or a Metaphor for Heterogeneity: From Single-Cell Analysis to Whole-Body Imaging. Biomedicines 12 (2024).
21. Stone, L.D. et al. Interim Phase II Results Using Panitumumab-IRDYE800CW during Transoral Robotic Surgery in Patients with Oropharyngeal Cancer. Clinical Cancer Research 30, 4016-4028 (2024).
22. Beffa, E.D. et al. Study protocol for Near-infrared molecular imaging for lung cancer detection and treatment during mini-invasive surgery (phase II Trial)-(the RECOGNISE study). BMC cancer 24, 1078 (2024).
23. Hamdy, F.C. et al. First-in-man study of the PSMA Minibody IR800-IAB2M for molecularly targeted intraoperative fluorescence guidance during radical prostatectomy. European Journal of Nuclear Medicine and Molecular Imaging 51, 3009-3025 (2024).
24. Vuijk, F.A. et al. Molecular targets for diagnostic and intraoperative imaging of pancreatic ductal adenocarcinoma after neoadjuvant FOLFIRINOX treatment. Sci Rep 10, 16211 (2020).
25. Awad, S., Alkashash, A.M., Amin, M., Baker, S.J. & Rose, J.B. Biochemical Predictors of Response to Neoadjuvant Therapy in Pancreatic Ductal Adenocarcinoma. Front Oncol 10, 620 (2020).
26. Versteijne, E. et al. Neoadjuvant Chemoradiotherapy Versus Upfront Surgery for Resectable and Borderline Resectable Pancreatic Cancer: Long-Term Results of the Dutch Randomized PREOPANC Trial. J Clin Oncol 40, 1220-1230 (2022).

SUPPLEMENTARY MATERIAL

All NMR and HPLC data of the compounds can be found at:
https://pubs.acs.org/doi/10.1021/acs.bioconjchem.5c00218?goto=supporting-info